Chemical Science

ROYAL SOCIETY OF CHEMISTRY

EDGE ARTICLE

View Article Online
View Journal | View Issue

Cite this: *Chem. Sci.*, 2024, **15**, 3893

All publication charges for this article have been paid for by the Royal Society of Chemistry

Received 14th December 2023
Accepted 2nd February 2024

DOI: 10.1039/d3sc06707f

rsc.li/chemical-science

Organocatalytic enantioselective synthesis of C_{sp_2}–N atropisomers *via* formal C_{sp_2}–O bond amination†

Chenxiao Qian,‡[ab] Jing Huang,‡[b] Tingting Huang,‡[a] Lijuan Song,[c] Jianwei Sun *[b] and Pengfei Li *[a]

Compared with well-developed construction of C_{sp_2}–C_{sp_2} atropisomers, the synthesis of C_{sp_2}–N atropisomers remains in its infancy, which is recognized as both appealing and challenging. Herein, we achieved the first organocatalyzed asymmetric synthesis of C_{sp_2}–N atropisomers by formal C_{sp_2}–O amination. With the aid of a suitable acid, 3-alkynyl-3-hydroxyisoindolinones reacted smoothly with 1-methylnaphthalen-2-ols to afford a wide range of atropisomers by selective formation of the C_{sp_2}–N axis. Particularly, both the kinetic (*Z*)-products and the thermodynamic (*E*)-products could be selectively formed. Furthermore, the rarely used combination of two chiral Brønsted acid catalysts achieved excellent enantiocontrol, which is intriguing and unusual in organocatalysis. Based on control experiments and DFT calculations, a cascade dehydration/addition/rearrangement process was proposed. More importantly, this work provided a new plat-form for direct atroposelective construction of the chiral C_{sp_2}–N axis.

Introduction

Atropisomers, the most widely recognized class of compounds featuring axial chirality, consist of conformers with restricted rotation around a single bond that enable their isolation in a stable form. In recent decades, significant advancements have been made in the construction of atropisomeric scaffolds, particularly with respect to highly developed C_{sp_2}–C_{sp_2} axis biaryls[1] and styrenes.[2] In stark contrast, despite the widespread occurrence of C–N axis in bioactive compounds[3] (Fig. 1A) and chiral ligands[4] (Fig. 1B), the catalytic asymmetric synthesis of these atropisomeric scaffolds is seldom reported due to their inherently less stable configuration and lower rotational barrier.[5] Traditional strategies for the construction of such enantioenriched frameworks rely on the functional group conversion of the existing C_{sp_2}–N axis,[6] such as *N*-functionalizations,[7] desymmetrizations,[8] asymmetric cyclizations.[9] Although central-to-axial chirality conversion can induce chiral C–N axes, it is not a one-step synthesis.[10] In this context, catalytic enantioselective construction of the C_{sp_2}–N axis is the most direct strategy, but this is also a highly challenging task that has been limitedly explored.

Currently, direct atroposelective construction of chiral C_{sp_2}–N axis mainly relies on two strategies: (i) organocatalytic asymmetric amination reactions, including electrophilic amination of electron-rich naphthalenes with azodicarboxylates/quinone diimines[11] and nucleophilic amination of azonaphthalenes with electron-rich amines[4c] (Scheme 1A); (ii) metal-catalyzed asymmetric coupling reactions of secondary amines with aryl halides[12] or diazo compounds[13] (Scheme 1B). In both scenarios, limited substrate scope and harsh reaction conditions constitute the major issues. Particularly, Lin *et al.*

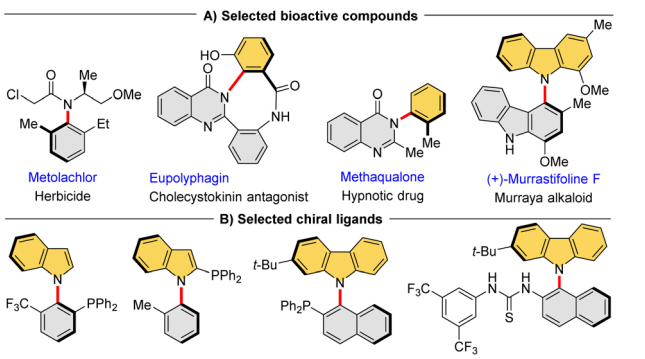

Fig. 1 Selected C–N atropisomeric compounds.

[a]*Department of Chemistry, Guangdong Provincial Key Laboratory of Catalysis, College of Science, Southern University of Science and Technology Guangming Advanced Research Institute, Southern University of Science and Technology (SUSTech), Shenzhen 518055, China. E-mail: lipf@sustech.edu.cn; flyli1980@gmail.com*

[b]*Department of Chemistry and the Hong Kong Branch of Chinese National Engineering Research Centre for Tissue Restoration & Reconstruction, The Hong Kong University of Science and Technology, Clear Water Bay, Kowloon, Hong Kong SAR, China. E-mail: sunjw@ust.hk*

[c]*School of Science, Harbin Institute of Technology (Shenzhen), Shenzhen 518055, China*

† Electronic supplementary information (ESI) available. For ESI and crystallographic data in CIF or other electronic format see DOI: https://doi.org/10.1039/d3sc06707f

‡ These authors contributed equally to this work.

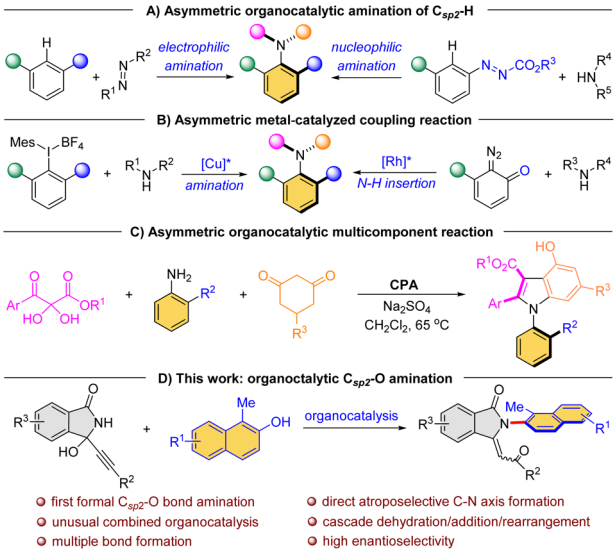

Scheme 1 Direct construction of C_{sp_2}–N atropisomers.

gracefully disclosed a chiral phosphoric acid (CPA)-catalyzed atroposelective cascade reaction among 2,3-diketoesters, aromatic amines and 1,3-cyclohexanediones for the construction of axially chiral *N*-arylindoles (Scheme 1C).[14] The reaction, however, still necessitated the utilization of dichloromethane at a temperature of 65 °C. Consequently, new efficient methods under mild conditions for the direct atroposelective construction of the C_{sp_2}–N bond remain in high demand.

It is known to be challenging to break a C_{sp_2}–O bond attached to electron-rich aromatic rings, as a result of the high C–O bond dissociation energy. Generally, transition metal catalysts, including Ni- and Pd-catalysts, are required for such C–O bond activation.[15] It is also known that aryl C–O bonds can be converted to C–N bonds with transition-metal-catalyzed catalysis, but no success has been achieved for direct construction of a chiral C_{sp_2}–N axis by C_{sp_2}–O bond activation.[16] Moreover, transition-metal-free amination often necessitates harsh conditions, such as high temperature and strong alkali.[17] Based on our previous research on indolinone derivatives[18] and in continuation of our efforts on the organocatalytic reactions of functionalized alcohols,[19] herein we discovered an intriguing dehydration/addition/rearrangement reaction between 1-substituted naphthols and indolinone derivatives leading to the formation of unusual C_{sp_2}–N atropisomeric scaffolds (Scheme 1D). More importantly, the catalytic asymmetric variant of this process has also been achieved by the combination of two chiral Brønsted acid catalysts.[20]

Results and discussion

We employed 1-methylnaphthalen-2-ol **1a** (ref. 21) and 3-alkynyl-3-hydroxyisoindolinone **2a** as the model substrates for this study. Initially, different Brønsted acids were chosen as catalysts in view of their proven performance (Table 1). In the presence of different sulfonic acids (**A1–A3**) and sufonimides (**A4–A5**) (Table 1, entries 1–5), two isomeric products (*Z*)-**3aa** and

Table 1 Condition optimization of the reaction between **1a** and **2a**

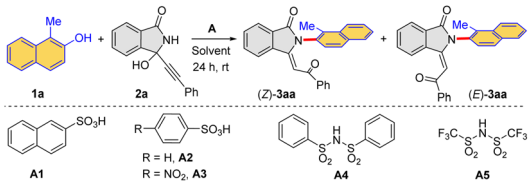

Entry[a]	A	Solvent	Yield [%][b]	
1	**A1**	CH_2Cl_2	(*Z*)-**3aa**, 63	(*E*)-**3aa**, 15
2	**A2**	CH_2Cl_2	(*Z*)-**3aa**, 10	(*E*)-**3aa**, 60
3	**A3**	CH_2Cl_2	(*Z*)-**3aa**, 14	(*E*)-**3aa**, 83
4	**A4**	CH_2Cl_2	(*Z*)-**3aa**, <5	(*E*)-**3aa**, <5
5	**A5**	CH_2Cl_2	(*Z*)-**3aa**, 10	(*E*)-**3aa**, 76
6	**A1**	MeCN	(*Z*)-**3aa**, <5	(*E*)-**3aa**, <5
7	**A1**	EtOAc	(*Z*)-**3aa**, 46	(*E*)-**3aa**, <5
8	**A1**	THF	(*Z*)-**3aa**, 22	(*E*)-**3aa**, <5
9	**A1**	CH_2Cl_2 (1.0 mL)	(*Z*)-**3aa**, 82	(*E*)-**3aa**, <5
10	**A1**	CH_2Cl_2 (1.2 mL)	(*Z*)-**3aa**, 90	(*E*)-**3aa**, <5
11	**A1**	CH_2Cl_2 (1.5 mL)	(*Z*)-**3aa**, 84	(*E*)-**3aa**, <5

[a] Unless noted, under Ar atmosphere, a mixture of **1a** (0.05 mmol), **2a** (0.10 mmol) and **A** (10 mol%) in the solvent (0.5 mL) was stirred at room temperature (rt) for 24 h. [b] Determined by ^{1}H NMR with CH_2Br_2 as internal standard.

(*E*)-**3aa** were observed, which contained a newly formed C_{sp_2}–N axis. Furthermore, it was also found that compound (*Z*)-**3aa** was the kinetic product, and the thermodynamic product (*E*)-**3aa** could be obtained from (*Z*)-**3aa** under the stronger Brønsted acidic conditions (details in mechanism studies). After careful screening of Brønsted acids, **A1** was identified as the optimal catalyst to obtain the product (*Z*)-**3aa** with a yield of 63% (Table 1, entry 1). Alternatively, **A3** could enable the formation of (*E*)-**3aa** with an improved yield of 83% (Table 1, entry 3). The further solvent evaluation revealed that CH_2Cl_2 was the optimal choice (Table 1, entries 6–8). Importantly, by adjusting substrate concentration, an improved yield of product (*Z*)-**3aa** was achieved (Table 1, entries 9–11).

Under the optimized conditions, the scope of the cascade dehydration/addition/rearrangement reaction between 1-methylnaphthalen-2-ols **1** and 3-alkynyl-3-hydroxyisoindolinones **2** was examined at a relatively larger scale. Because the target products (*Z*)-**3** could be converted to the thermodynamic products (*E*)-**3**, the time of each reaction was monitored by thin-layer chromatography (TLC). In some of these reactions, the amount of **A1** was increased to 20 mol% to shorten the reaction time to reduce isomerization. As shown in Table 2A, a range of naphthols **1a–j** reacted smoothly with 3-alkynyl-3-hydroxyisoindolinone **2a** to provide the corresponding (*Z*)-2-(naphthalen-2-yl)-isoindolin-1-ones (*Z*)-**3aa–ja** in moderate yields. These encouraging results indicated that the protocol could be applied to naphthols bearing different substituents, including trimethylsilyl ($SiMe_3$, Table 2, (*Z*)-**3ia**) and terminal olefin (Table 2, (*Z*)-**3ja**). In addition, the **A1**-catalyzed reaction also showed excellent compatibility with 3-alkynyl-3-hydroxyisoindolinones bearing different substituents in the

Table 2 Scope of reactions for (*Z*)-**3** and (*E*)-**3**

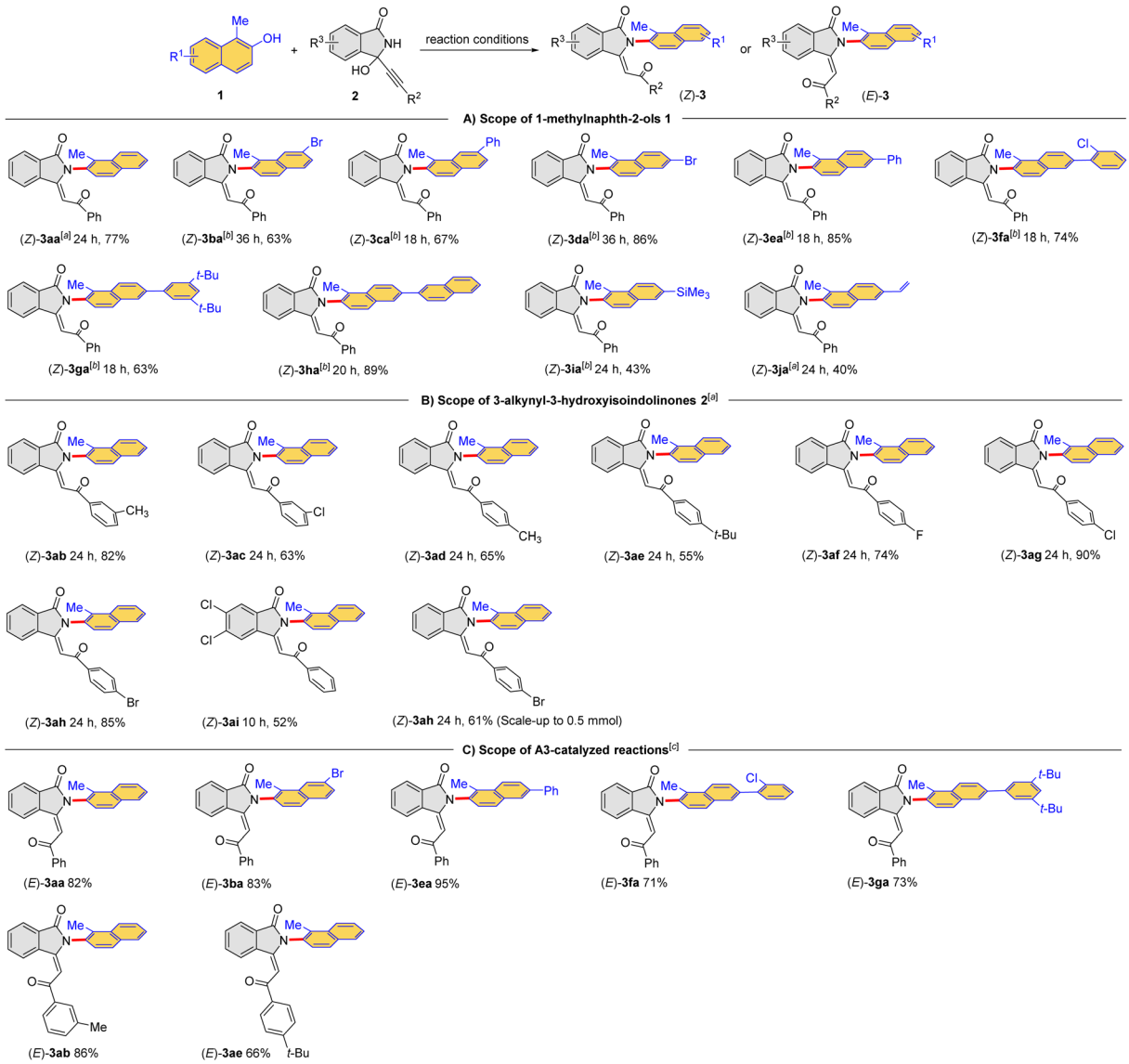

[a] A mixture of **1** (0.20 mmol), **2** (0.40 mmol) and **A1** (10 mol%) in CH_2Cl_2 (4.8 mL) was stirred at room temperature (rt) under Ar atmosphere for noted time. [b] A mixture of **1** (0.20 mmol), **2** (0.40 mmol) and **A1** (20 mol%) in CH_2Cl_2 (6.0 mL) was stirred at 30 °C under Ar atmosphere for the noted time. [c] A mixture of **1** (0.20 mmol), **2** (0.40 mmol) and **A3** (10 mol%) in CH_2Cl_2 (2.4 mL) was stirred at rt under Ar atmosphere for 24 h.

benzene ring, affording the desired products (*Z*)-**3ab–ah** in moderate to high yields (Table 2B). However, the methyl group in the 1-position of naphthol seemed to be essential. Replacing it by other substituents (H, Et) would lead to a complex mixture instead of desired product. The reaction of 1,3-dimethylnaphthalen-2-ol also resulted in the complex mixture. The configuration of (*Z*)-**3aa** was unambiguously confirmed by X-ray crystallography (CCDC 2294518). The configurations of other products were assigned by analogy.

The generality for the formation of the thermodynamic products (*E*)-**3** was also examined (Table 2C). Notably, the presented products were obtained in high yields after further optimizations. Exceptionally, some thermodynamic products were either formed in low efficiency or hard to isolated from the reaction mixture. The configuration of (*E*)-**3aa** was confirmed by X-ray crystallography (CCDC 2294530). Taken together, a divergent cascade reaction between 1-methylnaphthalen-2-ols and 3-alkynyl-3-hydroxyisoindolinones was achieved for the direct construction of C_{sp_2}–N bond from C_{sp_2}–O bond to furnish the kinetic products (*Z*)-**3** and the thermodynamic products (*E*)-**3**, respectively.

The successful construction of the C_{sp_2}–N axis inspired us to further develop an enantioselective variant of this process. Thus, the reaction between **1a** and **2a** was studied for the initial evaluation of some chiral phosphoric acids (Table 3, entries 1–2) and chiral phosphoramides (Table 3, entries 3–7) as potential

Table 3 Conditions optimization of the enantioselective reaction

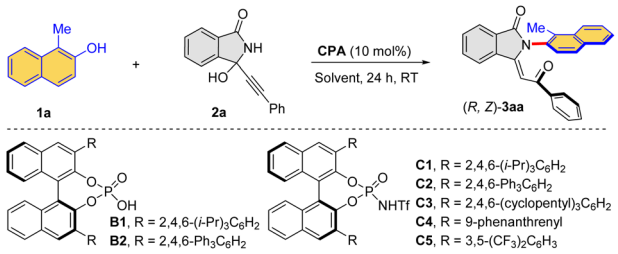

Entry[a]	CPA	Solvent	Temp [°C]	Yield [%][b]	ee [%][c]
1	**B1**	CH_2Cl_2	rt	Trace	—
2	**B2**	CH_2Cl_2	rt	Trace	—
3	**C1**	CH_2Cl_2	rt	64	65
4	**C2**	CH_2Cl_2	rt	20	46
5	**C3**	CH_2Cl_2	rt	44	53
6	**C4**	CH_2Cl_2	rt	Trace	—
7	**C5**	CH_2Cl_2	rt	18	7
8[d]	**C1/B1**	CH_2Cl_2	rt	40	61
9[e]	**C2/B2**	CH_2Cl_2	rt	34	90
10[f]	**C1/B2**	CH_2Cl_2	rt	44	90
11[f]	**C1/B2**	MeCN	rt	Trace	—
12[f]	**C1/B2**	EtOAc	rt	Trace	—
13[f]	**C1/B2**	THF	rt	Trace	—
14[g]	**C1/B2**	CH_2Cl_2	rt	44	90
15[h]	**C1/B2**	CH_2Cl_2	rt	32	88
16[g]	**C1/B2**	CH_2Cl_2	0	Trace	—
17[g,i]	**C1/B2**	CH_2Cl_2	rt to 0	56	93

[a] Unless noted, under Ar atmosphere, a mixture of **1a** (0.05 mmol), **2a** (0.10 mmol) and **CPA** (10 mol%) in the solvent (2.0 mL) was stirred at room temperature (rt) for 24 h. [b] Determined by ^{1}H NMR with CH_2Br_2 as internal standard. [c] Determined by chiral-HPLC analysis. [d] **C1** (10 mol%), **B1** (10 mol%). [e] **C2** (10 mol%), **B2** (10 mol%). [f] **C1** (10 mol%), **B2** (10 mol%). [g] **C1** (8 mol%), **B2** (8 mol%). [h] **C1** (5 mol%), **B2** (5 mol%). [i] The mixture was stirred at rt under Ar atmosphere for 5 min (**2a** was totally dissolved), then it was cooled to 0 °C for 6 days.

catalysts. Indeed, chiral phosphoramide **C1** was found to be a promising catalyst, affording the desired (*R*, *Z*)-**3aa** in 64% yield with 65% ee (Table 3, entry 3). While a single catalyst could not eventually improve the enantioselectivity to an excellent level, we were curious about the use of combined Brønstred acid systems. The combination of a chiral phosphoric acid and a chiral phosphoramide was then surveyed (Table 3, entries 8–10). Pleasingly, when phosphoramide **C1** was used together with chiral phosphoric acid **B2**, the desired (*R*, *Z*)-**3aa** was formed with 90% ee (Table 3, entry 10). Notably, control experiments indicated that the use of any other combination or any single acid could not reach such a high level of enantiocontrol. Other solvents could not improve the reaction outcome (Table 3, entries 11–13). Notably, the loading of **B2** and **C1** could be further reduced to 8.0 mol% without compromising the efficiency (Table 3, entry 14). No product was obtained when the reaction was carried out at 0 °C (Table 3, entry 16). It is worth noting that substrate **2a** has a low solubility at 0 °C. Therefore, a programmed cooling protocol was used to smoothly afford the target product (*R*, *Z*)-**3aa** with 93% ee (Table 3, entry 17).

Under the established conditions, the scope of this combined catalytic system was examined for this intriguing process for the direct formation of atroposelective C_{sp_2}–N axis (Table 4). The kinetic products (*R*, *Z*)-**3** were exclusively obtained under the optimized conditions. More specifically, a range of naphthols **1a–j** reacted smoothly with 3-alkynyl-3-hydroxyisoindolinone **2a** to provide the corresponding enantioenriched products (*R*, *Z*)-**3aa–ja** in moderate yields. The halogen (Br, Cl) could be introduced into the aromatic ring of naphthol, affording (*R*, *Z*)-**3ba–fa** in 32–68% yields with 79–92% ee. The reaction of naphthol with bulky substituents (3,5-(*t*-Bu)$_2$C$_6$H$_3$, 2-naphthyl) could also proceed smoothy, furnishing the corresponding products (*R*, *Z*)-**3ga** in 32% yield with 76% ee and (*R*, *Z*)-**3ha** in 64% yield with 94% ee, respectively. Particularly, trimethylsilyl and the terminal olefin unit were also compatible, and (*R*, *Z*)-**3ia** was obtained in 45% yield with 85% ee and (*R*, *Z*)-**3ja** in 40% yield with 94% ee. Moreover, a series of 3-alkynyl-3-hydroxyisoindolinones with different substituents (3-MeC$_6$H$_4$, 3-ClC$_6$H$_4$, 4-FC$_6$H$_4$, 4-ClC$_6$H$_4$, 4-BrC$_6$H$_4$) were also reactive to afford the desired products in generally moderate yields with high enantioselectivities. The reactions could be run at a relatively large scale (0.5 mmol), which afforded the desired products with comparable results as the small-scale reactions. The configuration of (*R*, *Z*)-**3aa** was confirmed by X-ray crystallography (CCDC 2294540).

To gain more information about the reaction mechanism, we have performed a series of control experiments. First of all, product (*Z*)-**3aa** could be converted to (*E*)-**3aa** in the presence of catalyst **A3**, which confirmed that the former is the kinetic product and the latter is the thermodynamic product (Scheme 2A).

Furthermore, no reaction took place between naphthalen-2-ol **1a** and enone **4** from 3-alkynyl-3-hydroxyisoindolinone **2a** under the standard conditions, suggesting that enone **4** was not a viable intermediate (Scheme 2B, eqn (1)). When $H_2{}^{18}O$ was added to the **A1**-mediated reaction, the ^{18}O atom was incorporated into the product (*Z*)-**3aa**-^{18}O (Scheme 2B, eqn (2)). Importantly, with 4 Å molecular sieves as additive, this process provided an allene as product, which was a mixture of diastereomers **IM-up** (weak polarity) and **IM-down** (strong polarity). The structure of this allene product was confirmed unambiguously by X-ray crystallography (CCDC 2294537, Scheme 2B, eqn (3)). Interestingly, the diastereomeric ratio (**IM-up** and **IM-down**) changed over time, likely *via* reverse reaction. Furthermore, with **B2** as catalyst, the allene diastereomers could be isolated as enantioenriched form (59% ee for **IM-up**, 39% ee for **IM-down**), both of which could lead to enantioenriched product (*R*, *Z*)-**3aa** in the presence of the racemic catalyst **C1** (Scheme 2B, eqn (4)), suggesting that the conversion from allene to product could be stereospecific. Moreover, the racemic allene diastereomers were also generated in the presence of catalyst A1 combined with 4 Å molecular sieves. Notably, treated with the combined catalysts, chiral **C1** and **B2**, enantioenriched (*R*, *Z*)-**3aa** could be still obtained (Scheme 2B, eqn (5)). We reasoned that, even though racemic, the allene intermediate could reverse to their precursors in the presence of the chiral acid to generate enantioenriched allene, which resulted in the

Table 4 Scope of reactions for (*R*, *Z*)-**3**[a]

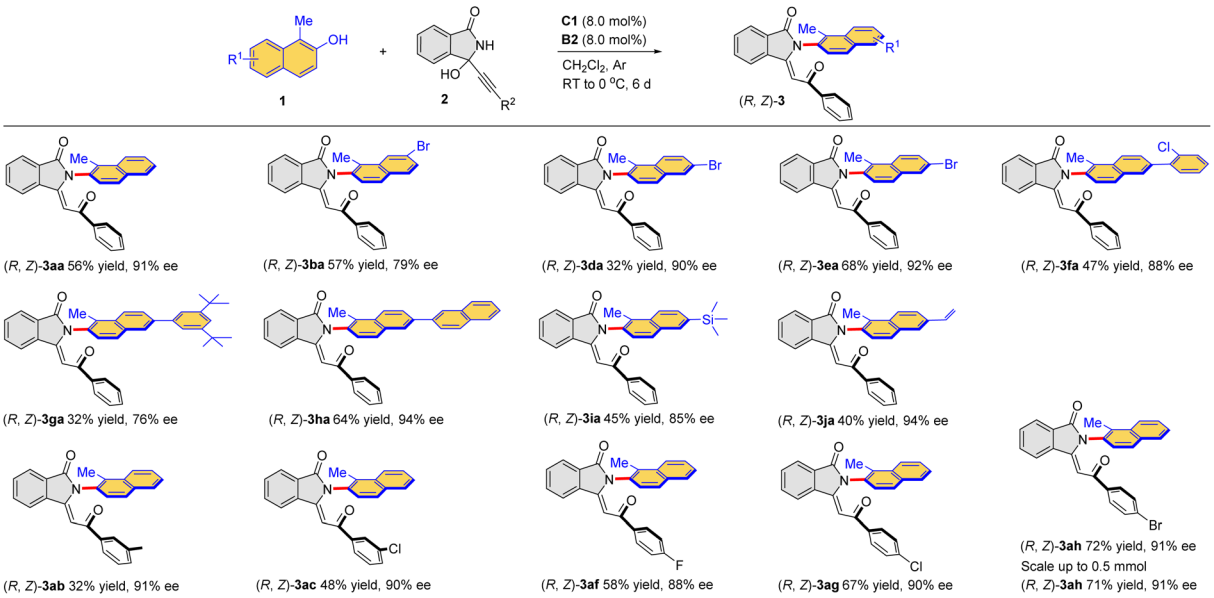

[a] Under Ar atmosphere, a mixture of **1** (0.20 mmol), **2** (0.40 mmol), **C1** (8 mol%) and **B2** (8 mol%) in CH_2Cl_2 (8.0 mL) was stirred at room temperature (rt) for 5 min, then it was cooled to 0 °C for 6 h. Products (*R*, *Z*)-**3** were obtained in isolated yields. The ee was determined by chiral-HPLC analysis.

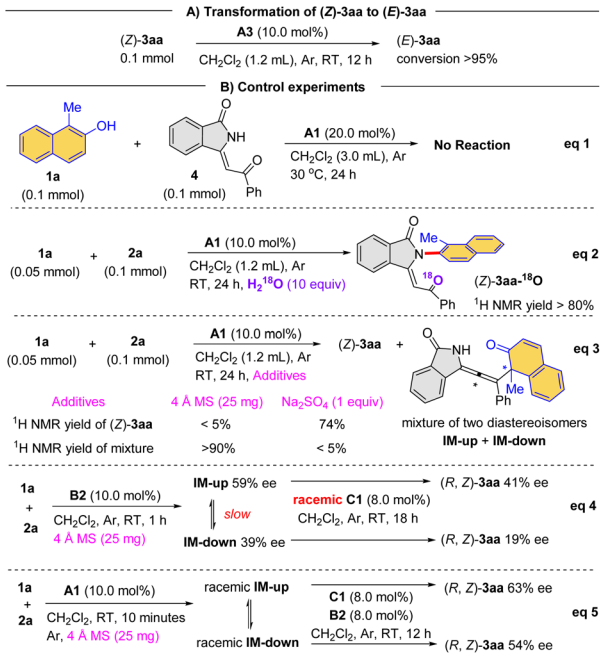

Scheme 2 Further investigations.

enantioenrichment in the final product. In this case, the rate-determining step is likely at a later stage (after allene formation), which would allow reversible steps before the addition of water to allene.

Interestingly, enantiopurity of product (*R*, *Z*)-**3aa** has a linear correlation to both the enantiopurity of **C1** (Scheme 3A) and **B2** (Scheme 3B), suggesting that both of them are contributing to the key enantiodetermining transition state. It is worth noting that such a scenario with two different chiral Brønsted acids contributing to enantiocontrol is extremely uncommon, to the best of our knowledge.

To understand the mechanism, density functional theory (DFT) calculations were performed on the racemic reaction. The results indicated that this intriguing process comprises of

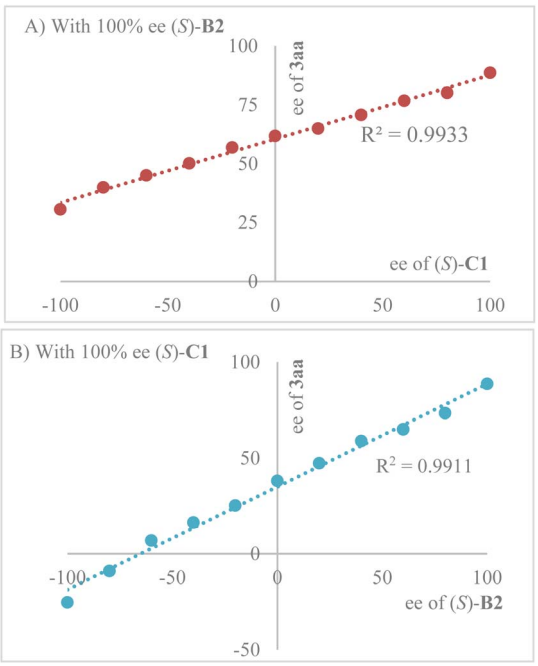

Scheme 3 Non-linear effect.

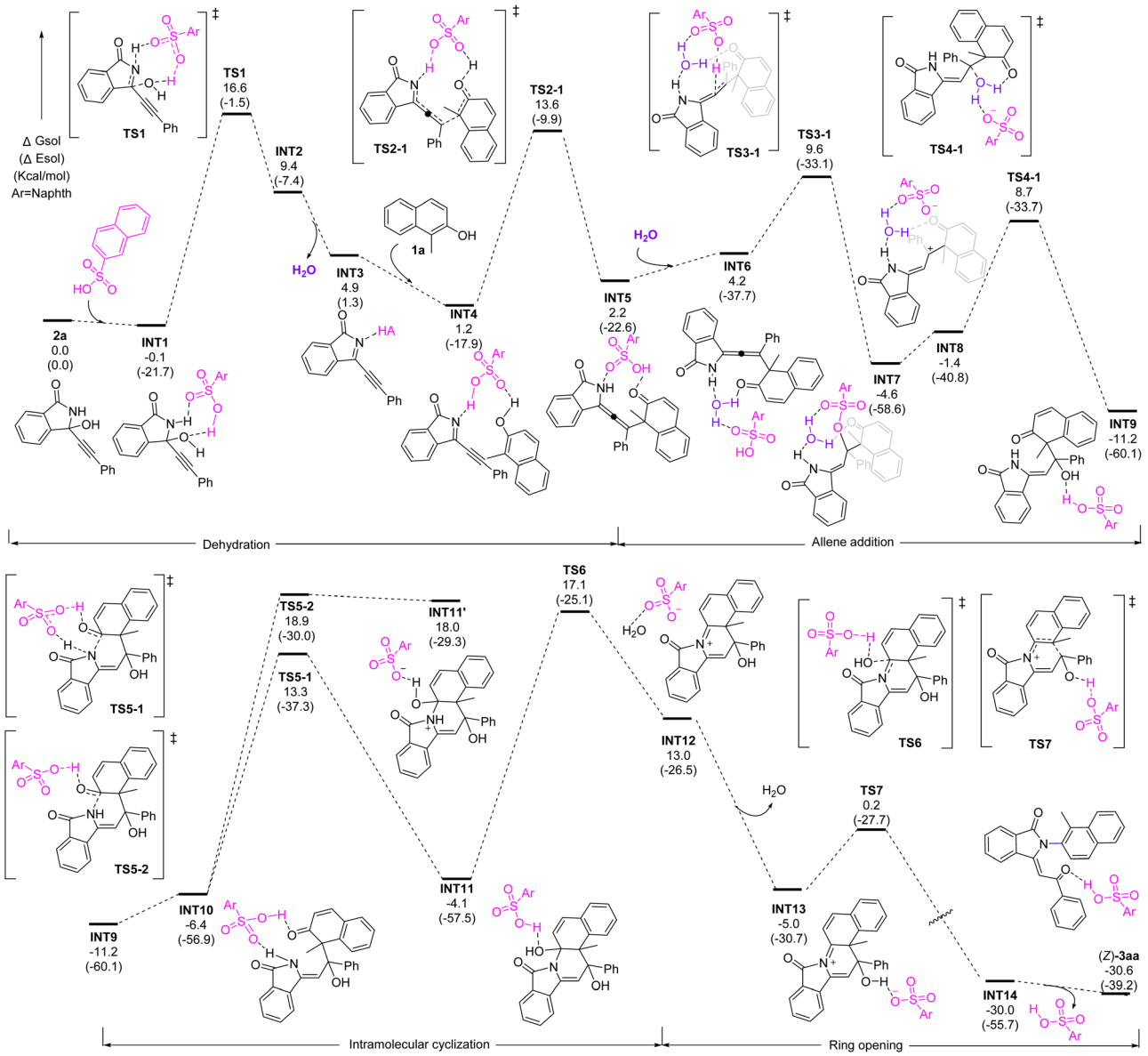

Fig. 2 DFT study. Energetic profiles of the reaction at the M06-2X-D3/6-311G(d,p)-SMD(DCM)//M06-2X-D3/6-31G(d) level of theory and the energy values are in given kcal mol^{-1}.

dehydration, allene formation, water addition, cyclization, and ring-opening (Fig. 2). It starts substrate coordination to naphthalene-2-sulfonic acid (**A1**) by hydrogen bonding followed by elimination of water to form intermediate **INT3** with an energy barrier of 16.7 kcal mol^{-1}. Next, a nucleophilic attack from the naphthol to the resulting imine **INT4** occurs together with synergistic proton transfer, leading to the allene intermediate **INT5**, with an energy barrier 12.4 kcal mol^{-1}. In the presence of water, the electron-rich allene motif can be further activated by acid and trigger a water addition to form **INT9**. Next, an intramolecular cyclization takes place by the nucleophilic attack of the N-atom to the carbonyl group to form a C–N bond. Further dehydration forms iminium **INT13**. Finally, a facile ring-opening process driven by the aromatization furnishes the final product. It is worth noting that the water elimination from **INT11** is the rate-determining step, which is consistent with the control experiments showing that the allene formation might be likely reversible.

Conclusions

In summary, we have successfully developed the first organocatalyzed asymmetric synthesis of C_{sp_2}–N atropisomers by formal C_{sp_2}–O amination. Different from known methods for the access to C_{sp_2}–N atropisomers by functionalization of existing C–N bonds, our process involved construction of the key C–N bond with concomitant asymmetric control. By adjusting the strength of the acid catalyst and reaction time, both the kinetic product (*Z*)-isomers and the thermodynamic product (*E*)-isomers could be selectively formed. More

importantly, the rarely used combination of two chiral Brønsted acid catalysts proved critical to the excellent enantiocontrol. Control experiments confirmed that both of them are required for the high enantioselectivity and both are involved in the enantiodetermining transition state. However, more accurate information about the enantiodetermining transition state is unknown at this point. DFT calculations also provided important information to the general reaction pathway, which involves allene as the key intermediate. Additional studies on this intriguing process are under-way in our laboratories.

Data availability

Experimental procedures, spectral data and DFT data can be found in the ESI.†

Author contributions

Pengfei Li, Jianwei Sun and Chenxiao Qian wrote the manuscript. Pengfei Li and Jianwei Sun supervised the project. Pengfei Li conceived the project. Chenxiao Qian and Tingting Huang performed condition optimization, scope study and control experiments. Jing Huang and Lijuan Song performed DFT studies. All the authors proofread and commented on the manuscript.

Conflicts of interest

There are no conflicts to declare.

Acknowledgements

The authors acknowledge the financial support from Shenzhen Innovation of Science and Technology Commission (20200925151614002), Guangdong Innovative Program (2019BT02Y335), and Guangdong Provincial Key Laboratory of Catalysis (2020B121201002). The authors acknowledge the assistance of SUSTech Core Research Facilities, Xiaoyong Chang (X-ray), and Yang Yu (HRMS).

Notes and references

1 Selected reviews, see: (*a*) G. Bringmann, A. J. P. Mortimer, P. A. Keller, M. J. Gresser, J. Garner and M. Breuning, *Angew. Chem., Int. Ed.*, 2005, **44**, 5384–5427; (*b*) J. Wencel-Delord, A. Panossian, F. R. Leroux and F. Colobert, *Chem. Soc. Rev.*, 2015, **44**, 3418–3430; (*c*) Y.-B. Wang and B. Tan, *Acc. Chem. Res.*, 2018, **51**, 534–547; (*d*) M. I. Lapuh, S. Mazeh and T. Besset, *ACS Catal.*, 2020, **10**, 12898–12919; (*e*) H.-H. Zhang and F. Shi, *Acc. Chem. Res.*, 2022, **55**, 2562–2580; (*f*) J. K. Cheng, S.-H. Xiang and B. Tan, *Acc. Chem. Res.*, 2022, **55**, 2920–2937.

2 Selected reports, see: (*a*) S.-C. Zheng, S. Wu, Q. Zhou, L. W. Chung, L. Ye and B. Tan, *Nat. Commun.*, 2017, **8**, 15238–15245; (*b*) Y.-B. Wang, P. Yu, Z.-P. Zhou, J. Zhang, J. Wang, S.-H. Luo, Q.-S. Gu, K. N. Houk and B. Tan, *Nat. Catal.*, 2019, **2**, 504–513; (*c*) L. Jin, Q.-J. Yao, P.-P. Xie, Y. Li, B.-B. Zhan, Y.-Q. Han, X. Hong and B.-F. Shi, *Chem*, 2020, **6**, 497–511; (*d*) C. Ma, F.-T. Sheng, H.-Q. Wang, S. Deng, Y.-C. Zhang, Y. Jiao, W. Tan and F. Shi, *J. Am. Chem. Soc.*, 2020, **142**, 15686–15696.

3 (*a*) G. Chesters, G. V. Simsiman, J. Levy, B. J. Alhajjar, R. N. Fathulla and J. M. Harkin, *Rev. Environ. Contam. Toxicol.*, 1989, **110**, 1–74; (*b*) H.-L. Jiang, X.-H. Luo, X.-Z. Wang, J.-L. Yang, X.-J. Yao, P. Crews, F. A. Valeriote and Q.-X. Wu, *Fitoterapia*, 2012, **83**, 1275–1280; (*c*) Y.-B. Wang, S.-C. Zheng, Y.-M. Hu and B. Tan, *Nat. Commun.*, 2017, **8**, 15489–15497.

4 (*a*) T. Mino, S. Komatsu, K. Wakui, H. Yamada, H. Saotome, M. Sakamoto and T. Fujita, *Tetrahedron: Asymmetry*, 2010, **21**, 711–718; (*b*) T. Mino, M. Ishikawa, K. Nishikawa, K. Wakui and M. Sakamoto, *Tetrahedron: Asymmetry*, 2023, **24**, 499–504; (*c*) W. Xia, Q.-J. An, X.-H. Xiang, S. Li, Y.-B. Wang and B. Tan, *Angew. Chem., Int. Ed.*, 2020, **59**, 6775–6779.

5 Selected reviews, see: (*a*) T.-Z. Li, S.-J. Liu, W. Tan and F. Shi, *Chem. – Eur. J.*, 2020, **26**, 15779–15792; (*b*) O. Kitagawa, *Acc. Chem. Res.*, 2021, **54**, 719–730; (*c*) G.-J. Mei, W. L. Koay, C.-Y. Guan and Y. Lu, *Chem*, 2022, **8**, 1855–1893; (*d*) J. Feng, C.-J. Lu and R.-R. Liu, *Acc. Chem. Res.*, 2023, **56**, 2537–2554.

6 Selected reviews, see: (*a*) G. Bringmann, T. Gulder, T. A. M. Gulder and M. Breuning, *Chem. Rev.*, 2011, **111**, 563–639; (*b*) E. Kumarasamy, R. Raghunathan, M. P. Sibi and J. Sivaguru, *Chem. Rev.*, 2015, **115**, 11239–11300; (*c*) Y.-J. Wu, G. Liao and B.-F. Shi, *Green Synth. Catal.*, 2022, **3**, 117–136; (*d*) S. Choppin and J. Wencel-Delord, *Acc. Chem. Res.*, 2023, **56**, 189–202.

7 Selected reports, see: (*a*) O. Kitagawa, M. Kohriyama and T. Taguchi, *J. Org. Chem.*, 2002, **67**, 8682–8684; (*b*) J. Terauchi and D. P. Curran, *Tetrahedron: Asymmetry*, 2003, **14**, 587–592; (*c*) O. Kitagawa, M. Takahashi, M. Yoshikawa and T. Taguchi, *J. Am. Chem. Soc.*, 2005, **127**, 3676–3677; (*d*) O. Kitagawa, M. Yoshikawa, H. Tanabe, T. Morita, M. Takahashi, Y. Dobashi and T. Taguchi, *J. Am. Chem. Soc.*, 2006, **128**, 12923–12931; (*e*) S. Shirakawa, K. Liu and K. Maruoka, *J. Am. Chem. Soc.*, 2012, **134**, 916–919; (*f*) S.-L. Li, C. Yang, Q. Wu, H.-L. Zheng, X. Li and J.-P. Cheng, *J. Am. Chem. Soc.*, 2018, **140**, 12836–12843; (*g*) G.-H. Yang, H. Zheng, X. Li and J.-P. Cheng, *ACS Catal.*, 2020, **10**, 2324–2333.

8 Selected reports, see: (*a*) D. P. Curran, H. Qi, S. J. Geib and N. C. DeMello, *J. Am. Chem. Soc.*, 1994, **116**, 3131–3132; (*b*) W.-L. Duan, Y. Imazaki, R. Shintani and T. Hayashi, *Tetrahedron*, 2007, **63**, 8529–8536; (*c*) J.-W. Zhang, J.-H. Xu, D.-J. Cheng, C. Shi, X.-Y. Liu and B. Tan, *Nat. Commun.*, 2016, **7**, 10677–10686; (*d*) L.-L. Zhang, J.-W. Zhang, S.-H. Xiang, Z. Guo and B. Tan, *Org. Lett.*, 2018, **20**, 6022–6026; (*e*) C. Parida, S. K. Dave, K. Das and S. C. Pan, *Adv. Synth. Catal.*, 2023, **365**, 1185–1190.

9 Selected reports, see: (*a*) K. Tanaka, K. Takeishi and K. Noguchi, *J. Am. Chem. Soc.*, 2006, **128**, 4586–4587; (*b*) H. Liu, W. Feng, C. W. Kee, D. Leow, W.-T. Loh and C.-H. Tan, *Adv. Synth. Catal.*, 2010, **352**, 3373–3379; (*c*) N. Ototake, Y. Morimoto, A. Mokuya, H. Fukaya, Y. Shida

and O. Kitagawa, *Chem. – Eur. J.*, 2010, **16**, 6752–6755; (*d*) T. Li, C. Mou, P. Qi, X. Peng, S. Jiang, G. Hao, W. Xue, S. Yang, L. Hao, Y. R. Chi and Z. Jin, *Angew. Chem., Int. Ed.*, 2021, **60**, 9362–9367; (*e*) Q.-J. An, W. Xia, W.-Y. Ding, H.-H. Liu, S.-H. Xiang, Y.-B. Wang, G. Zhong and B. Tan, *Angew. Chem., Int. Ed.*, 2021, **60**, 24888–24893.

10 (*a*) C. Sun, X. Qi, X.-L. Min, X.-D. Bai, P. Liu and Y. He, *Chem. Sci.*, 2020, **11**, 10119–10126; (*b*) V. Corti, M. K. Thøgersen, V. J. Enemærke, N. M. Rezayee, C. L. Barløse and K. A. Jørgensen, *Chem. – Eur. J.*, 2022, **28**, e202202395.

11 (*a*) S. Brandes, M. Bella, A. Kjærsgaard and K. A. Jørgensen, *Angew. Chem., Int. Ed.*, 2006, **45**, 1147–1151; (*b*) S. Brandes, B. Niess, M. Bella, A. Prieto, J. Overgaard and K. A. Jørgensen, *Chem. – Eur. J.*, 2006, **12**, 6039–6052; (*c*) H.-Y. Bai, F.-X. Tan, T.-Q. Liu, G.-D. Zhu, J.-M. Tian, T.-M. Ding, Z.-M. Chen and S.-Y. Zhang, *Nat. Commun.*, 2019, **10**, 3063–3071; (*d*) J. Qin, T. Zhou, T.-P. Zhou, L. Tang, H. Zuo, H. Yu, G. Wu, Y. Wu, R.-Z. Liao and F. Zhong, *Angew. Chem., Int. Ed.*, 2022, **61**, e202205159.

12 (*a*) J. Rae, J. Frey, S. Jerhaoui, S. Choppin, J. Wencel-Delord and F. Colobert, *ACS Catal.*, 2018, **8**, 2805–2809; (*b*) J. Frey, A. Malekafzali, I. Delso, S. Choppin, F. Colobert and J. Wencel-Delord, *Angew. Chem., Int. Ed.*, 2020, **59**, 8844–8848.

13 (*a*) Q. Ren, T. Cao, C. He, M. Yang, H. Liu and L. Wang, *ACS Catal.*, 2021, **11**, 6135–6140; (*b*) C. Niu, Y. Zhou, Q. Chen, Y. Zhu, S. Tang, Z.-X. Yu and J. Sun, *Org. Lett.*, 2022, **24**, 7428–7433.

14 L. Wang, J. Zhong and X. Lin, *Angew. Chem., Int. Ed.*, 2019, **58**, 15824–15828.

15 S.-Q. Zhang and X. Hong, *Acc. Chem. Res.*, 2021, **54**, 2158–2171.

16 Z. Qiu and C.-J. Li, *Chem. Rev.*, 2020, **120**, 10454–10515.

17 X. Chang, Q. Zhang and C. Guo, *Org. Lett.*, 2019, **21**, 4915–4918.

18 (*a*) C. Qian, M. Liu, J. Sun and P. Li, *Org. Chem. Front.*, 2022, **9**, 1234–1240; (*b*) C. Qian, T. Huang, J. Sun and P. Li, *Org. Lett.*, 2022, **24**, 6472–6476; (*c*) Y. Xia, M. Liu, C. Qian, P. Li, M. Dong and W. Li, *Org. Chem. Front.*, 2023, **10**, 30–34.

19 (*a*) S. Liu, K. L. Chan, Z. Lin and J. Sun, *J. Am. Chem. Soc.*, 2023, **145**, 12802–12811; (*b*) M. Liu, B. Shen, C. Liu, P. Yu and P. Li, *J. Am. Chem. Soc.*, 2023, **145**, 14562–14569.

20 For pioneering examples of CPA catalysis, see: (*a*) T. Akiyama, J. Itoh, K. Yokota and K. Fuchibe, *Angew. Chem., Int. Ed.*, 2004, **43**, 1566–1568; (*b*) D. Uraguchi and M. Terada, *J. Am. Chem. Soc.*, 2004, **126**, 5356–5357; (*c*) D. Nakashima and H. Yamamoto, *J. Am. Chem. Soc.*, 2006, **128**, 9626–9627; (*d*) D. Parmar, E. Sugiono, S. Raja and M. Rueping, *Chem. Rev.*, 2014, **114**, 9047–9153; (*e*) T. Akiyama and K. Mori, *Chem. Rev.*, 2015, **115**, 9277–9306; (*f*) T. James, M. van Gemmeren and B. List, *Chem. Rev.*, 2015, **115**, 9388–9409; (*g*) J. Kikuchi and M. Terada, *Chem. – Eur. J.*, 2021, **27**, 10215–10225.

21 A. B. Woldegiorgis, Z. Han and X.-F. Lin, *Org. Lett.*, 2021, **23**, 6606–6611.